Hindawi
International Journal of Chemical Engineering
Volume 2023, Article ID 8887905, 15 pages
https://doi.org/10.1155/2023/8887905

Research Article

Optimization of Mechanical Properties and Surface Characteristics of PLA+ 3D Printing Materials

Ali H. Kadhum, Salah Al-Zubaidi, and Salah Sabeeh Abed AlKareem

Department of Automated Manufacturing Engineering, Al-Khwarizmi College of Engineering, University of Baghdad, Baghdad 10071, Iraq

Correspondence should be addressed to Salah Al-Zubaidi; salah.salman@kecbu.uobaghdad.edu.iq

Received 10 March 2023; Revised 23 June 2023; Accepted 4 August 2023; Published 21 August 2023

Academic Editor: Andreas Bück

Recently, there is a growing demand towards adopting 3D printing technology in various sectors due to its potential merits. The mechanical properties and surface quality of the final product are influenced by the process parameters. Therefore, this study aims to optimize the infill density and pattern beside printing speed and temperature to achieve optimum mechanical properties and surface characteristics of PLA+ 3D-printed material. The Taguchi method was applied with L9 array, and tensile and surface roughness tests were carried out to evaluate the performance of specimens in terms of the obtained ultimate tensile strength, Young's modulus, tensile strain (%), and surface roughness. The selected parameters with their levels were as follows: printing temperature (205, 215, and 225°C), printing speed (20, 50, and 80 mm/s), infill density (30%, 60%, and 90%), and infill pattern (triangle, cubic, and concentric). The findings revealed the significant impact of the infill density followed by the infill pattern on the mechanical and surface performances of the PLA+ material. From the other side, the Taguchi method was integrated with grey relational analysis (GRA) as a multiobjective optimization to find out the optimum mechanical properties and surface characteristics of the 3D-printed PLA+ part. Accordingly, 215°C, 50 mm/s, 90%, and triangle pattern achieved optimum mechanical properties (24 MPa, 3.14 GPa, and 13.72%) and surface roughness (3.21 μm).

1. Introduction

Recently, additive manufacturing (AM) attracts many researchers and manufacturers to investigate and utilize this promising technology [1]. Many merits are provided by AM that enlarge demand for this process such as improving productivity, producing intricate parts, and minimizing warehouses and waste materials [2, 3]. Also, a wide range of materials and techniques can be employed in the AM. Accordingly, this technology has found a good market in many sectors such as automotive, defense, medical, and aerospace due to its flexibility compared with conventional technologies [4–7]. In general, some traditional manufacturing processes involve material removal (as in metal cutting processes) to produce the desired geometry of the machined part. Therefore, annually industrial sectors in various fields lose a huge amount of materials in the form of chips. In contrast, additive manufacturing adds materials through a layering process to produce the required part with dimensions according to the specification [8]. Fused deposition modeling (FDM) is one of the most applied additive manufacturing (AM) processes, in which melted filament is extruded through a nozzle and deposited on the platform to produce layered products immediately from the part CAD model [9]. FDM is applied in different areas, particularly the biomedical sector, to process prostheses, implants, drugs, etc. [10]. FDM process utilizes various kinds of thermoplastic filaments with round cross-sections such as polylactic acid (PLA), improved polylactic acid (PLA+), polyethylene terephthalate glycol (PETG), and acrylonitrile butadiene styrene (ABC). PLA biodegradable material is processed from grown plants, including corn, cassava, and potato, using bacterial fermentation [11]. PLA+ is a modified version of PLA with good impact resistance and adherence between printed layers, making it suitable for 3D printing functional products. It demonstrated its potential as biomaterials in various medical applications, including

cardiovascular implants, regenerative medicine or tissue engineering, orthopedic treatments, cancer therapy, dental specialties, drug carriers, skin and tendon mending, and medical equipment and tools [12, 13].

The bonding between two successive layers on the print platform occurs in FDM at four different stages as follows: contact between surfaces, growth of neck, diffusion interface, and randomizing [14].

Optimization plays a vital role in manufacturing as well as almost other sectors [15]. A set of works have been published previously in the field of 3D printing parametric and optimization studies. The most studied response of the final 3D-printed product was mechanical properties. Some parameters were studied by the researchers in the literature besides printing temperature and speed like raster angle, infill density (%), infill pattern, and layer height. The raster angle refers to the angle confined between the deposited raster path and the axes of the base platform. The infill density stands for the volume of deposited material inside the part being 3D printed. The geometry and structure of the deposited material inside the part represent the infill pattern. The layer height is the thickness of the individual successive deposited layer. For instance, the infill density (%), printing temperature, raster angle, and layer height have been examined by Leite [16] to show their impact on the obtained ultimate tensile strength (σu), Young's modulus (E), elongation%, and toughness of PLA tensile specimens. Twenty-four experimental runs were carried out and the results were analyzed statistically by using analysis of variance (ANOVA). The mechanical properties of ABS 3D-printed parts were improved via optimizing the layer thickness and infill pattern by using the Taguchi approach [17]. Physical and mechanical properties of four resins were investigated by Christian and Ezekielle [18]. The ultimate tensile and bending strengths were evaluated.

The PLA filaments are preferred over ABS ones [19] in terms of strength and stiffness and 3D printability, but both are most popular 3D-printed materials and considered by previous studies [20–22].

The mechanical properties of some 3D-printed materials were investigated by Tanikella et al. [23]. The external and internal textures of the 3D-printed specimens were tested to find out the best layer height taken into account, the specimen mass, and extrusion variables. The mechanical properties of PLA material were verified with the findings of the finite element simulation [24]. Also, Lubombo and Huneault [25] investigated the PLA mechanical properties at low infill density. The performance of PLA material was improved in terms of mechanical and electrical properties by reinforcement with carbon nanoparticles (CNPs) [26]. The influence of different percentages of infill density and printing orientation of PLA+ specimens were also studied [27]. In another study, the impact of printing angles and volume fraction of wood-PLA filament composite were assessed based on the obtained mechanical properties [28]. 25% of wood filaments were more effective on the mechanical properties of the produced composite.

A fused deposition modeling was applied to 3D print of PLA at printing speed, temperature, number of layers, and thickness of 200 mm/s, 200°C, 30 layers, and 0.2 mm, respectively [29]. The specimens were printed with grid, trihexagon, triangle, and quarter cubic patterns at 60% infill density and have been examined with compression and low rate impact tests. Grid pattern gained 72 MPa as maximum compression strength, while triangle structure made impact resistance and Young's modulus to reach 7.5 J and 0.68 GPa. The infill structures have been optimized by using the topology optimization method [30–32]. The findings recommended the use of gradient as optimum infill instead of fixed distance ones where it maintained better mechanical properties and reduced printing time.

Also, the infill pattern and other 3D printing parameters were optimized by another work [33]. The printed samples showed significant difference in terms of tensile and bending strengths based on the applied pattern, speed, orientation, and feed rate. The PLA was strengthened with ammonium perchlorate by printing with FMD technology using complex and combustible patterns [34]. The study demonstrated the performance of energetic and structural processed composite. A cubic specimen of PLA was printed at 20–60% infill density to examine its response to different densities in terms of printing time where 60% produced higher value of 227 min [35]. The higher strength of 3D-printed work part was achieved by the correct tuning of printing orientation and raster angle for different 3D-printed materials [36].

According to the cited works, little attention was paid to the optimization of the mechanical and surface qualities of the 3D-printed PLA+ material by using a multiobjective optimization scheme. Therefore, the current study attempts to optimize the mechanical properties and surface characteristics of 3D PLA+ material by using the integrated Taguchi–grey relational analysis (GRA) method as a multiobjective optimization.

2. Materials and Procedures

PLA+ filaments were printed by using 3D printer in the form of tensile test specimen according to the ASTM-D628 standard. The PLA+ filament with diameter of 1.75 mm was provided by the Hello 3D Chinese company. The total number of printed specimens was 9 according to the applied Taguchi method with L9 orthogonal array.

Taguchi's design of experiment is a powerful tool capable of reducing the cycle time of design and manufacturing stages. At the same time, it enables us to identify the significant controllable parameters that influence the process through the analysis of variance (ANOVA). Furthermore, it is a systematic and easy-to-apply method that provides a minimum and sufficient number of experiments for the investigated case study in which the time is saved and the cost of experiments is reduced [37, 38].

According to the Taguchi method, two different tracks were suggested for problem analysis [37] as follows:

(1) Analysis of variance (ANOVA).

(2) Signal-to-noise ratio (S/N).

ANOVA evaluates the significance of one or more parameters by comparing their variables' output response means at various parameter levels. On the other hand, the S/N ratio determines the response variability concerning the target value subjecting to different noise conditions.

For the maximization problem (higher is better), equation (1) is applied to calculate the maximum response. While equation (2) is used for the minimization problem (smaller is better). In the current study, the target is maximizing the ultimate tensile strength (σu), Young's modulus (E), and tensile strain of the 3D-printed PLA+ material. In contrast, it is targeted to minimize the surface roughness of the same material as follows:

$$\eta = -10\log_{10}\left[\frac{1}{n}\sum_{i=1}^{n}\frac{1}{y_i^2}\right], \quad (1)$$

$$\eta = -10\log_{10}\left[\frac{1}{n}\sum_{i=1}^{n}y_i^2\right], \quad (2)$$

where η, y_i, and n denote the S/N ratio, experiment (i), and experiment's total number, respectively.

In the current study, the Taguchi experimental design scheme with L9 orthogonal array was applied using Minitab-17 statistical software. Therefore, nine specimens were printed by using 3D printer (model Ender3 Pro), as shown in Figure 1. The thermoplastic filaments that are utilized in FDM must have a circular cross-section, as stated above. The printer has a digital display to select and choose the appropriate printing parameters. The extruder has two wheels, namely, a tensioner and a feeder to guide the filament towards the thermal chamber for heating to a predetermined temperature over the melting point and then extruding via the nozzle onto a glass platform. The feeder is typically attached to the stepper motor, which powers this process. The tensioner grasps the filament. The thermal chamber is supplied with a heater having a thermocouple to carry out the heating and maintain the desired temperature. The nozzle throat is encased in a heat sink to avoid filament melting before entering the thermal chamber. It dissipates heat from the nozzle head to avoid potential extruder clogging. The cooling fan accelerates the dissipation of heat from the nozzle opening. Additional stepper motors are fixed to tune the extrusion track of melted filament on the driven platform, which moves downward in the Z-direction during the layer-building process [39].

The standard tensile specimens were printed under four printing parameters with three levels each as illustrated in Table 1. The factors A, B, C, and D stand for four printing parameters, namely, printing temperature (°C), printing speed (mm/min), infill density (%), and infill pattern. The levels of these parameters were chosen with equal interval. When applying the Taguchi approach with L9 orthogonal array using the parameters and their levels in Table 1, Table 2 is constructed.

The surface roughness in terms of Ra was measured by using stylus roughness tester prior the tensile test. The mechanical properties of PLA+ were determined by carrying out the tensile test using universal tensile test machine. The ultimate tensile strength (σu), Young's modulus (E), and tensile strain were calculated directly from the plotted stress-strain curves of the nine specimens.

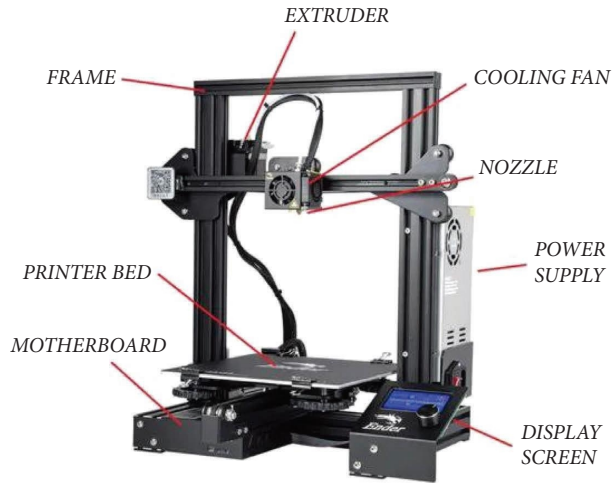

Figure 1: 3D printer model Ender3 pro.

3. Results and Discussion

The results of mechanical properties and surface roughness of PLA+ 3D-printed specimens are collected and presented in the table and curve form as depicted in Table 3 and Figure 2. These tables and curves will be subjected to statistical, parametric, and optimization analysis in this section. The aims are to determine the degree of significance for the developed statistical model and its corresponding factors and their contributions in the production of the output response, to conduct parametric analysis for the influence of printing parameters on the mechanical and surface properties of the 3D-printed specimens, and finally, to find out the optimum 3D printing settings which generate higher mechanical properties and finer surface roughness.

3.1. Statistical and Parametric Analysis of 3D Printing of PLA+ Materials. To perform statistical and parametric analysis, it is so important to construct and present the ANOVA results and the main effect plots of the mean. Thus, Tables 4–7 illustrate the ANOVA results for the ultimate tensile strength (σu), Young's modulus of elasticity (E), tensile strains (ε) (%), and Ra, respectively.

The DF, Adj SS, Adj MS, F-value, and P value terminologies of the ANOVA Tables 4–7 represent the degree of freedom, adjusted square error, adjusted mean square, F, and P values, respectively. The degree of freedom refers to the amount of the informative data of the model. The following formulas are used to calculate the degree of freedom for the following: regression model, each factor, error, and ad total as follows:

Table 1: 3D printing parameters and levels.

3D-printing parameter	Parameters in coded form	Levels		
		Low	Medium	High
Printing temperature (°C)	A	205	215	225
Printing speed (mm/min)	B	20	50	80
Infill density (%)	C	30	60	90
Infill pattern	D	Triangle	Cubic	Concentric

Table 2: Experimental matrix.

No.	Printing temperature (°C)	Printing speed (mm/s)	Infill density (%)	Infill pattern
1	205	20	30	Triangle
2	205	50	60	Cubic
3	205	80	90	Concentric
4	215	20	60	Concentric
5	215	50	90	Triangle
6	215	80	30	Cubic
7	225	20	90	Cubic
8	225	50	30	Concentric
9	225	80	60	Triangle

Table 3: Experimental results of the mechanical properties for PLA+ specimens.

No.	Printing temperature (°C)	Printing speed (mm/s)	Infill density (%)	Infill pattern	Ultimate tensile strength σu (MPa)	Young's modulus E (GPa)	Tensile strain ε (%)	Ra (μm)
1	205	20	30	Triangle	16	2.26	17.25	2.05
2	205	50	60	Cubic	19	2.60	12.75	2.78
3	205	80	90	Concentric	23	3.22	11.63	3.81
4	215	20	60	Concentric	18	2.58	16.88	2.91
5	215	50	90	Triangle	24	3.14	13.72	3.21
6	215	80	30	Cubic	15	2.17	14.18	3.63
7	225	20	90	Cubic	23	3.11	9.66	2.45
8	225	50	30	Concentric	15	2.09	16.25	3.11
9	225	80	60	Triangle	20	2.66	15.89	3.31
		Min			15	2.09	9.66	2.05
		Max			24	3.22	17.25	3.81

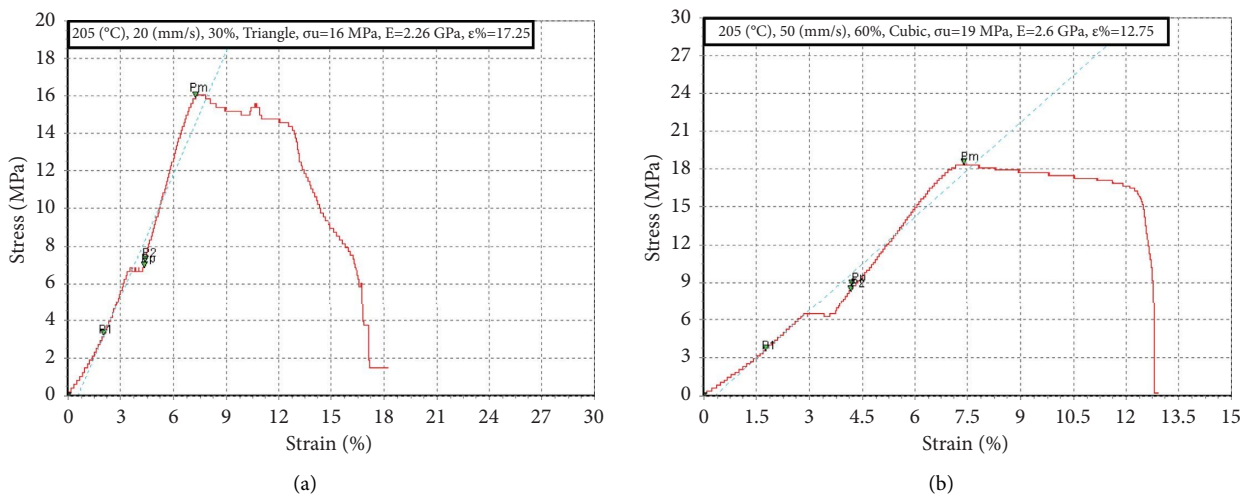

(a) (b)

Figure 2: Continued.

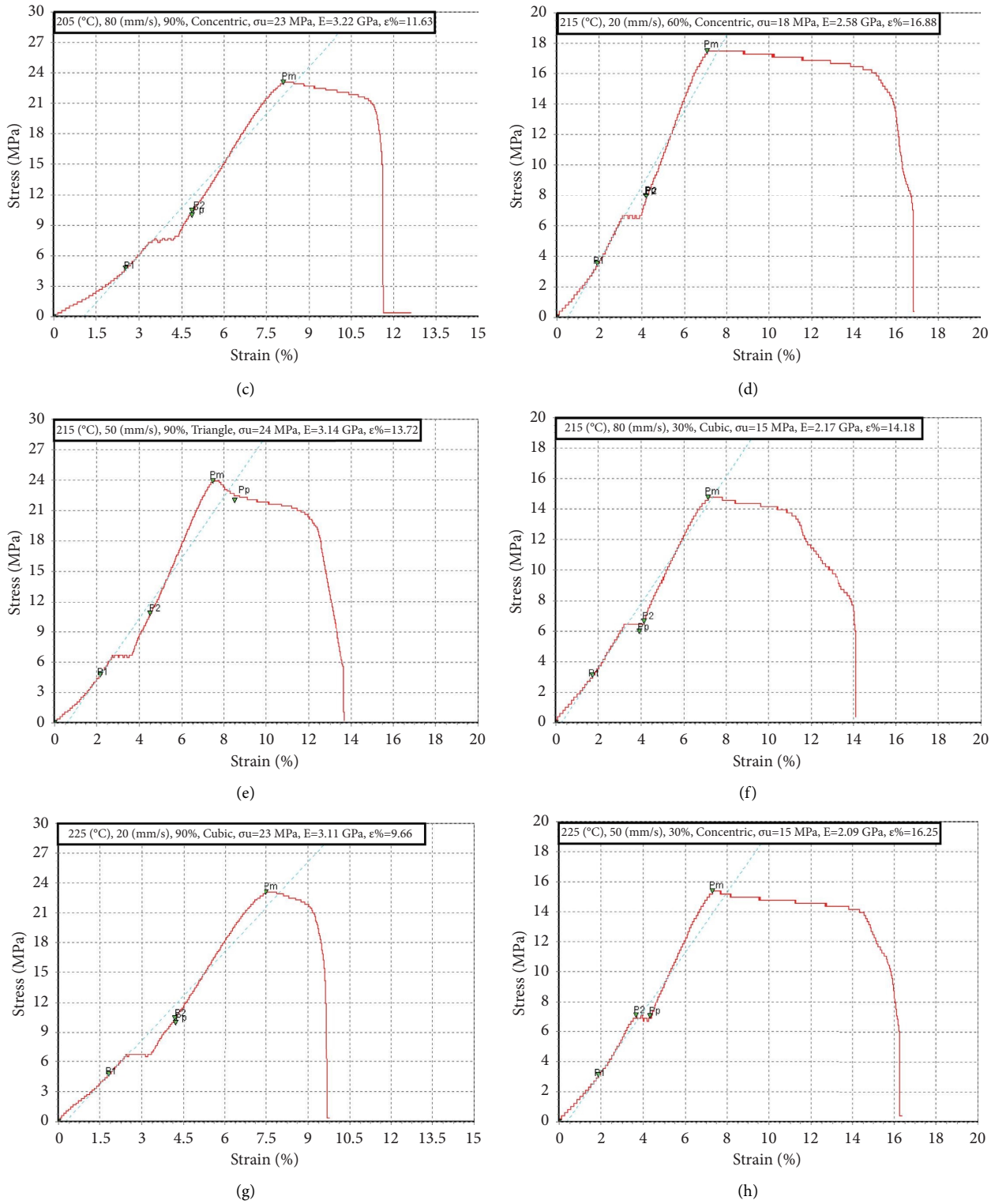

Figure 2: Continued.

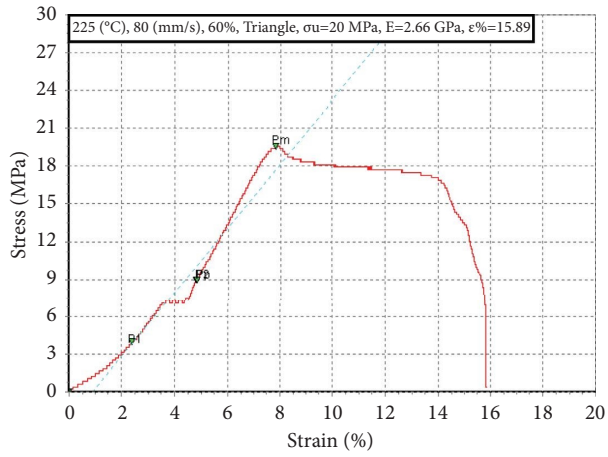

(i)

Figure 2: Stress-strain curves of PLA+ 3D-printed materials (specimens (a)–(i)).

Table 4: ANOVA results of ultimate tensile strength (σu) (MPa).

Source	DF	Adj SS	Adj MS	*F*-value	*P* value	Rank
Regression	4	96.1667	32.0556	47.30	0.001	—
Temperature (A)	1	0.0000	0.0000	0.001	1.000	4
Speed (B)	1	0.1667	0.1667	0.25	0.641	3
Infill density (%) (C)	1	96.0000	96.0000	141.64	0.001	1
Infill pattern (D)	1	0.22913	0.22913	0.48	0.527	2
Error	4	3.3889	0.6778			—
Total	8	99.78473				—

Table 5: ANOVA results of Young's modulus of elasticity (*E*) (GPa).

Source	DF	Adj SS	Adj MS	*F*-value	*P* value	Rank
Regression	4	1.57230	0.39308	103.52	0.001	—
Temperature (A)	1	0.00807	0.00807	2.12	0.219	4
Speed (B)	1	0.00167	0.00167	0.44	0.544	3
Infill density (%) (C)	1	1.55042	1.55042	408.30	0.001	1
Infill pattern (D)	1	0.01215	0.01215	3.20	0.148	2
Error	4	0.01519	0.00380			—
Total	8	1.58749				—

Table 6: ANOVA results of tensile strain (ε) (%).

Source	DF	Adj SS	Adj MS	*F*-value	*P* value	Rank
Regression	4	28.8570	7.2142	1.14	0.0452	—
Temperature (A)	1	0.5192	0.5192	0.08	0.789	4
Speed (B)	1	0.8288	0.8288	0.13	0.736	3
Infill density (%) (C)	1	26.8605	26.8605	4.24	0.109	1
Infill pattern (D)	1	0.6485	0.6485	0.10	0.765	2
Error	4	25.3530	6.3382			—
Total	8	54.2099				—

Table 7: ANOVA results of surface roughness (Ra).

Source	DF	Adj SS	Adj MS	F-value	P value	Rank
Regression	4	2.21342	0.55336	8.83	0.029	—
Temperature (A)	1	0.00814	0.00814	0.13	0.737	4
Speed (B)	1	1.86484	1.86484	29.74	0.005	1
Infill density (%) (C)	1	0.07752	0.07752	1.24	0.328	3
Infill pattern (D)	1	0.26292	0.26292	4.19	0.110	2
Error	4	0.25079	0.06270			—
Total	8	2.46421				—

$$\begin{aligned}\text{degree of freedom (DF) of regression model} &= \text{no. of factors} = m = 4,\\ \text{degree of freedom (DF) of each factor} &= 1,\\ \text{degree of freedom (DF) of error} &= n - m - 1 = 9 - 4 - 1 = 4,\\ \text{total degree of freedom (DF)} &= n - 1 = 8,\end{aligned} \tag{3}$$

where n = no. of experiments = 9 and m = no. of factors = 4.

The adjusted square error (Adj SS) determines the variation of the model's different factors. The adjusted mean square (Adj MS) measures all the factor variations of the model. The F-value is a statistical measure that identifies whether model factors correlate with the output response. A larger F-value means the significance of the model or factor. The probability of P value determines the strength of the data supporting the null hypothesis. More substantial evidence is presented against the null hypothesis via lower probabilities. If the P value is less than the significance level (0.05), then the model or term is significant, and vice versa.

The following equations are used by Minitab software to calculate Adj SS and Adj MS as follows:

$$\text{adj ss of regression} = n\sum_{j=1}^{4}\left(x_j - \overline{x}\right)2, \tag{4}$$

where n = size of sample for group j x_j, which is mean of group (j) $\overline{x}$ = the overall mean of the four group as follows:

$$\text{adj ss of error} = \sum_{j=1}^{4}\sum_{i=1}^{3}\left(x_{\text{ij}} - \overline{x_j}\right)2, \tag{5}$$

where x_{ij} is the i^{th} experimental run within group (j) and $\overline{x_j}$ is the mean of group (j) as follows:

$$\begin{aligned}\text{total adj ss} &= \text{adj ss of regression} + \text{adj ss of error},\\ \text{adj MS} &= \frac{\text{adj ss}}{\text{DF}}.\end{aligned} \tag{6}$$

With respect to Table 4 of ultimate tensile strength (σu), it is obvious that the model is significant with P value quite less than 0.05 at 95% confidence level. Thus, the model can be navigated and enabled for the purpose of studying of its controllable factors. Another point is the factors recorded different P values depending on their degree of significance. Therefore, only the infill density (%) was the significant factor that impacted the ultimate tensile strength (σu) with high percentage of contribution. Two more things have to be mentioned here, which are R-sq and contribution percentage of the factors. Excellent R-sq of 96.6% was achieved and the contribution percentage of the printing temperature, speed, infill density (%), and pattern were as follows: 0.0033%, 0.167%, 96%, and 0.23%, respectively. In other words, the large contribution came from the infill density.

Similarly, the ANOVA Table 5 confirms the significance of the Young modulus model as well as the effect of infill density (%) based on the achieved P values. Other factors were also not registered a degree of significance. 99.09% was obtained as R-sq, while printing temperature, speed, infill density, and pattern contributed with the following: 0.508%, 0.1052%, 97.665%, and 0.7654%. Pertaining to the ANOVA of the tensile strength of Table 6, the model is significant but the printing factors are not. Anyhow, the infill density (%) is still more influenced than other factors where it recorded a contribution percentage of 49.549% followed by printing speed (1.5289%), infill pattern (1.1963%), and finally printing temperature (0.9578%). The achieved R-sq was 89.86%, and it is considered as an acceptable percentage.

Finally, ANOVA results of surface roughness (Ra) were found in Table 7. The significance of the model is confirmed through the low P value (0.029) and at the same time, the table indicates the effect of the printing speed on the surface roughness. Conversely, other factors did not record any significance due to relatively large P values, but the infill pattern was more influence factor compared with temperature and infill density (%). Good R-sq value was achieved for surface roughness with 89.82%. Also, the order of contributors was as follows: printing speed, infill density pattern, infill density (%), and temperature with contribution percentages as follows: 75.677%, 10.67%, 3.146%, and 0.33%, respectively. These contributions are compatible with the corresponding F-values. It is noticed that the factors rank is added to Tables 4–7, and this rank was in the same order for the printing parameters and for all responses (i.e., ultimate tensile strength (σu), Young's modulus (E), tensile strain (%), and surface roughness (Ra)). For all outputs, the infill density (%) keeps the class one because it was more influential and contributing factor to the output responses. The statistical findings support and attribute to the trend of

achieved results in terms of the effect of 3D printing parameters on the four responses.

Figure 2 illustrates P1, P2, and Pm beside the plateau zone. P1 and P2 points refer to the first and second point of yielding as provided with tester software, while Pm represents the maximum achieved strength, which stands for the ultimate tensile strength. The PLA+ is semicrystalline material that has crystalline and amorphous regions. The plateau zone in Figure 2 is attributed to unstable crystalline area during tension that work as buffer field that restrict stress rising and therefore create plateau area.

Figures 3–6 give an illustration about how the four responses are affected by the printing factors, where A = printing temperature (°C), B = printing speed (mm/s), C = infill density (%), and D = infill pattern. For instance, in Figure 3, the impact of infill density (%) is visible compared with other factors where large strengths were recorded at 90% density. From the other side, the average strength for each parameter level is near to the mean value of nine runs due to their low contributions.

The stiffness of the PLA+ specimens was also highly affected by the infill density (%) in contrast with infill pattern, printing temperature, and speed, as depicted in Figure 4. The trend of the mean effect plot for Young's modulus (E) is similar to that of the ultimate tensile strength (σu).

Regarding the main effect plot for the tensile strain (ε) (%), it can be noticed that the infill density influence is reverse to the corresponding behaviors of the ultimate tensile strength (σu) and Young's modulus of elasticity (E), as shown in Figure 5.

This means that increasing the infill density gives noticeable reduction in tensile strain (ε) (%). Also, infill pattern reveals visible impact particularly triangle pattern. Other two factors (i.e., temperature and speed) did not show significant contribution to the tensile strain (ε) (%).

Finally, the surface roughness (Ra) is subjected to more coarsening due to the increase in the printing speed, infill density (%), and infill pattern with different levels unlike printing temperature, which produce slight increase in the roughness at low and medium levels and return back to the lower value at a high-level temperature, as shown in Figure 6.

To sum up, the 3D-printing parameters affected the four responses with different levels and various contribution percentages. However, the most effective parameter that impacted the first three responses was the infill density (%) from the point of view of ultimate tensile strength (σu), and increasing the infill density (%), which means increasing of solid fraction on the account of empty fraction inside the cross-section area of the reduced section for the tensile specimen. In other words, the applied stress must be larger to reach the ultimate tensile strength (σu) and ended with necking and fracture. From the other side, increasing the infill density promotes the chance of increasing stiffness by empowering of bonding between layers and molecules. Also, setting the more influencing parameter on the low level gives more probability to increase the change in the length over the original gauge length in which the tensile strain increases. At the end, the surface roughness was influenced greatly with the printing speed than other parameters where fine surface texture was produced at this speed with less valleys and waviness.

3.2. Optimization of the 3D-Printing Parameters. In the previous section, a statistical and parametric analysis of the main findings was performed to highlight the reliability of the developed model in terms of its significance and their corresponding factors, contribution percentages (%), R-sq, and factor rank order. This section undertakes the optimization of 3D-printing parameters to identify the optimum mechanical and surface properties of the PLA+ material.

The Taguchi method was applied in this section as single objective optimization to optimize the mechanical properties and surface roughness of the PLA+ materials separately. The larger is better was selected as the target for the mechanical properties, while smaller is better was chosen for the surface roughness.

Each of the low printing temperature (A1), high printing speed (B3), high infill density (C3), and triangle pattern (D1) delivered a highest signal to noise ratio, as illustrated by Figure 7. In other words, the optimum setting that may maintain maximum ultimate tensile strength (σu) is 205°C, 80 mm/s, 90%, and the triangle pattern.

Investigation of Figure 8 reveals that the optimum printing parameters that ensure maximum Young's modulus of elasticity (E) are similar to those that yielded the highest ultimate tensile strength (σu): A1, B3, C3, and D3 (i.e., 205°C, 80 mm/s, 90%, and triangle pattern).

Medium printing temperature and printing speed (A2 and B2) with low infill density (%) and triangle pattern (C1 and D1) may keep the tensile strain at the maximum value. Therefore, they represent the optimum parameters for maximum tensile strain where they produced the highest signal to noise ratio as depicted in Figure 9.

At the end, placing the printing temperature, printing speed, infill density (%), and pattern on the low levels (A1, B1, C1, and D1), as shown in Figure 10, sustains the fine surface roughness because these levels achieved large signal-to-noise ratio that enable the producing of fine surface.

To sum up and give more illustrative view about the optimized setting of the 3D printing parameters, Table 8 is constructed. This table presents the optimized printing parameters for each response independently. In other words, each response has its own independent optimized settings because the Taguchi method is a single optimization method.

4. Multiobjective Optimization of 3D-Printing Parameters of PLA+ Materials

In the preceding section, the 3D-printing parameters were optimized for each response separately. That means the optimum parameters for mechanical and surface properties are different for response to response. The Taguchi method suffers from demerits that it solves only single objective optimization problem. The current study has four dependent responses that rely on four independent input parameters. Therefore, these input parameters have to be optimized to find out the combined optimum mechanical and surface characteristics. In other words, the problem will be multiobjective optimization.

To perform such task, the Taguchi approach was integrated with grey relational analysis (GRA) to provide an

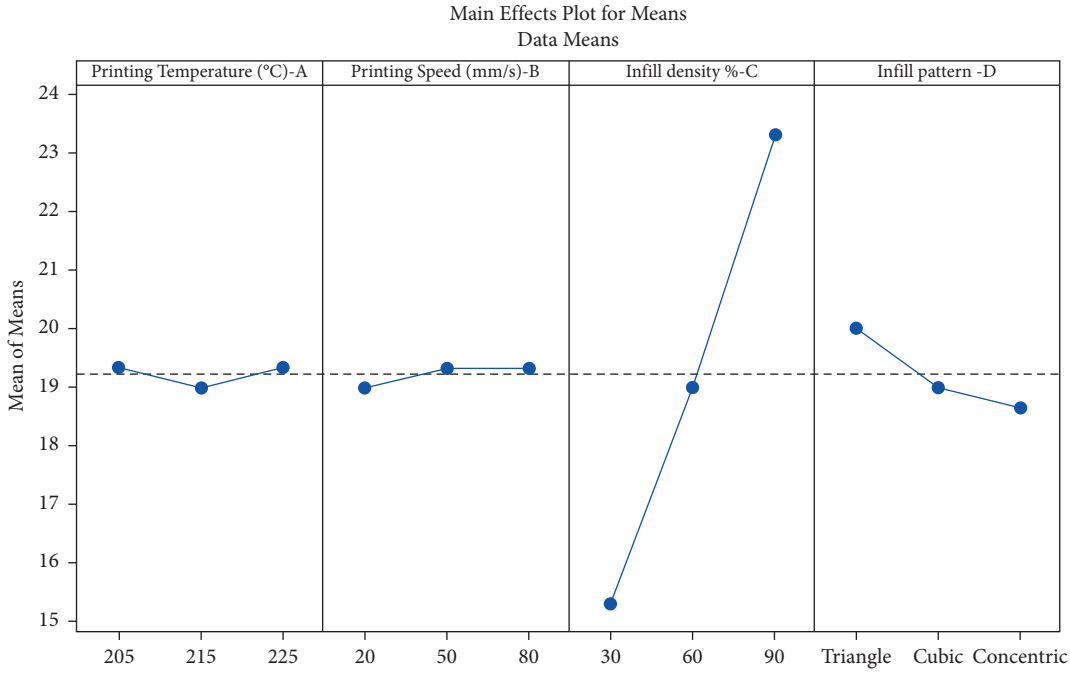

Figure 3: Main effect plot for the means of ultimate tensile strength (σu).

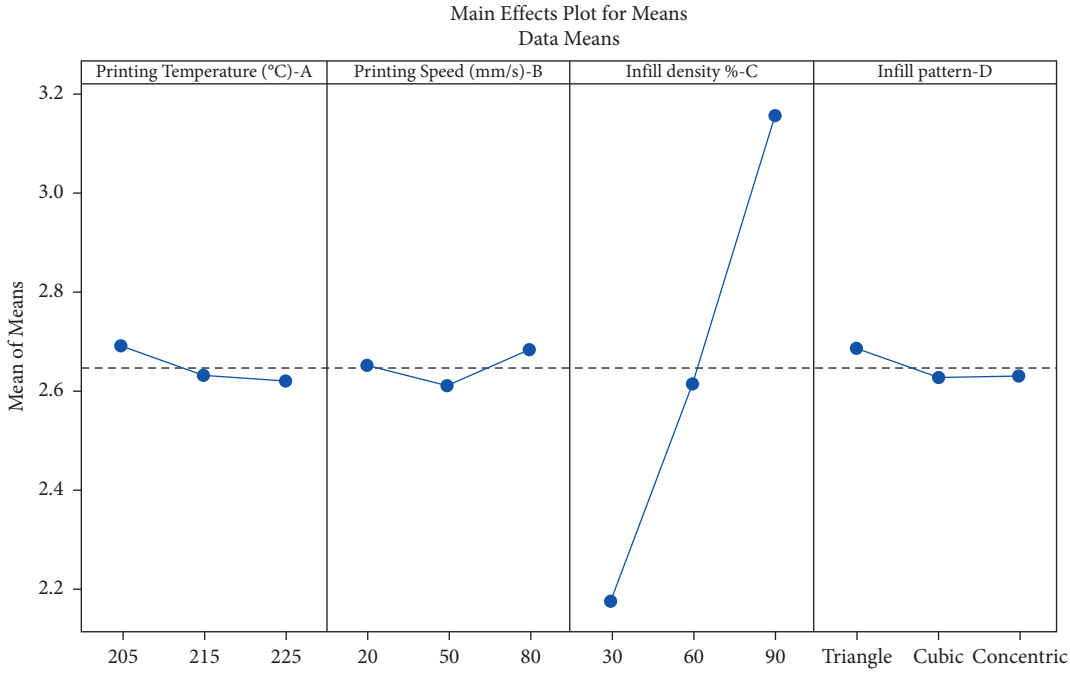

Figure 4: Main effect plot for means of the Young's modulus (E).

optimum solution for the mechanical and surface characteristics of the PLA+ materials.

This approach transforms multiresponse to single response optimization [40, 41]. It involves different steps that must be carried out sequentially to reach the optimized settings. Among them are the following:

(i) Normalization of all responses

(ii) Finding the grey relational coefficients (GRCs)

(iii) Determining the grades of grey relational analysis

Larger is better is chosen for the mechanical properties, while smaller is better is selected for surface roughness. The normalization is preprocessing step aims to limit the responses values between 0 and 1 and convert original response to comparable one. The mechanical responses (ultimate tensile strength, Young's modulus of elasticity, and tensile strain) is normalized by using equation (7), while

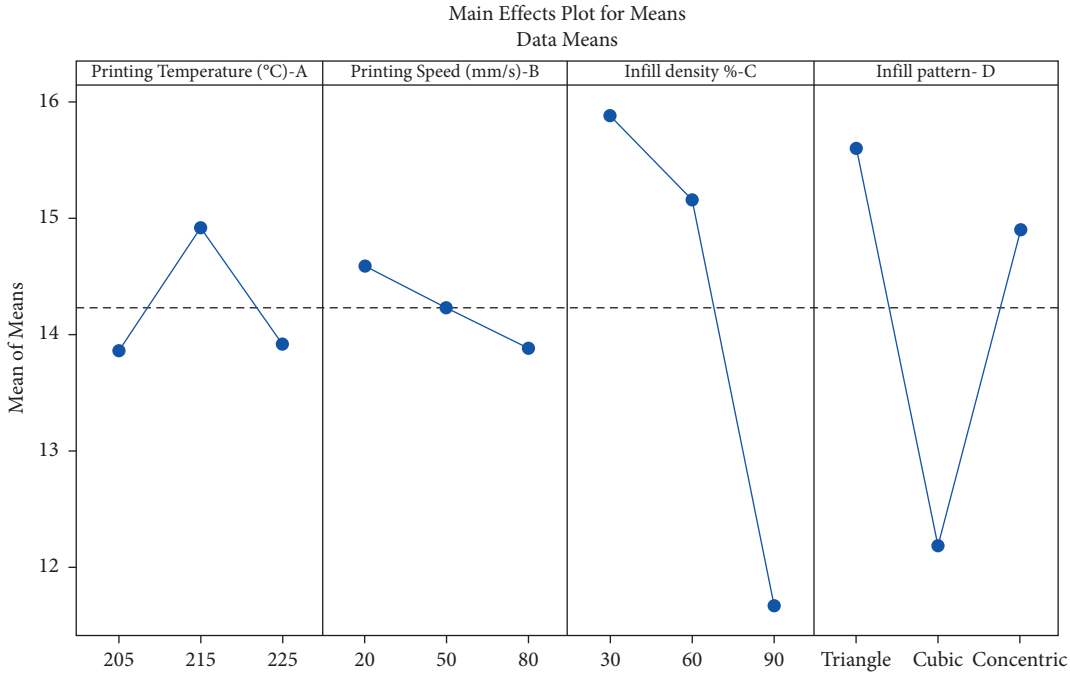

Figure 5: Main effect plot for the means of the tensile strain (%).

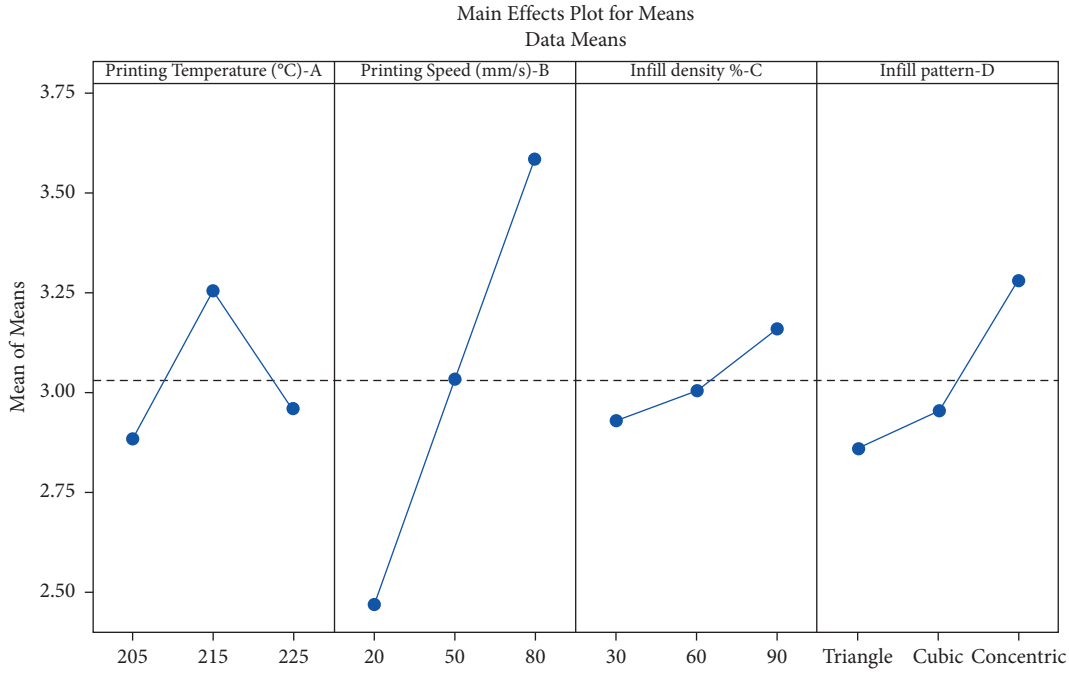

Figure 6: Main effect plot for means of the surface roughness.

equation (8) is used to normalize the surface roughness response because it is selected as smaller is better.

$$x(k) = \frac{y_i(k) - \min y_i(k)}{\max y_i(k) - \min y_i}, \quad (7)$$

$$x_i(k) = \frac{\max y_i(k) - y_i(k)}{\max y_i(k) - \min y_i(k)}, \quad (8)$$

where $x_i(k)$ = grey relational normalized value of i^{th} run and k^{th} response, $\min y_i(k)$ = lowest value of $y_i(k)$ for k^{th} response, and $\max y_i(k)$ = highest value of the $y_i(k)$ for the k^{th} response.

The two formulas are the same shared dominators with different numerators because the first one stand for larger is better while second formula is used for smaller is better. Applying the equations (7) and (8) on experimental data in

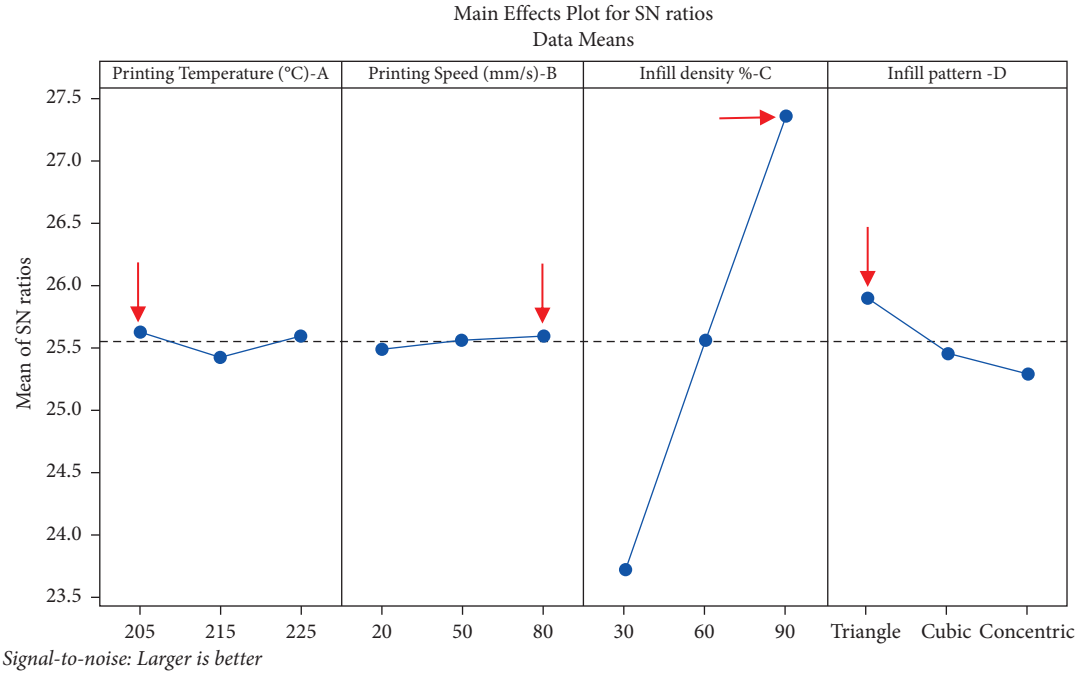

Figure 7: S/N plot of the ultimate tensile strength (σu).

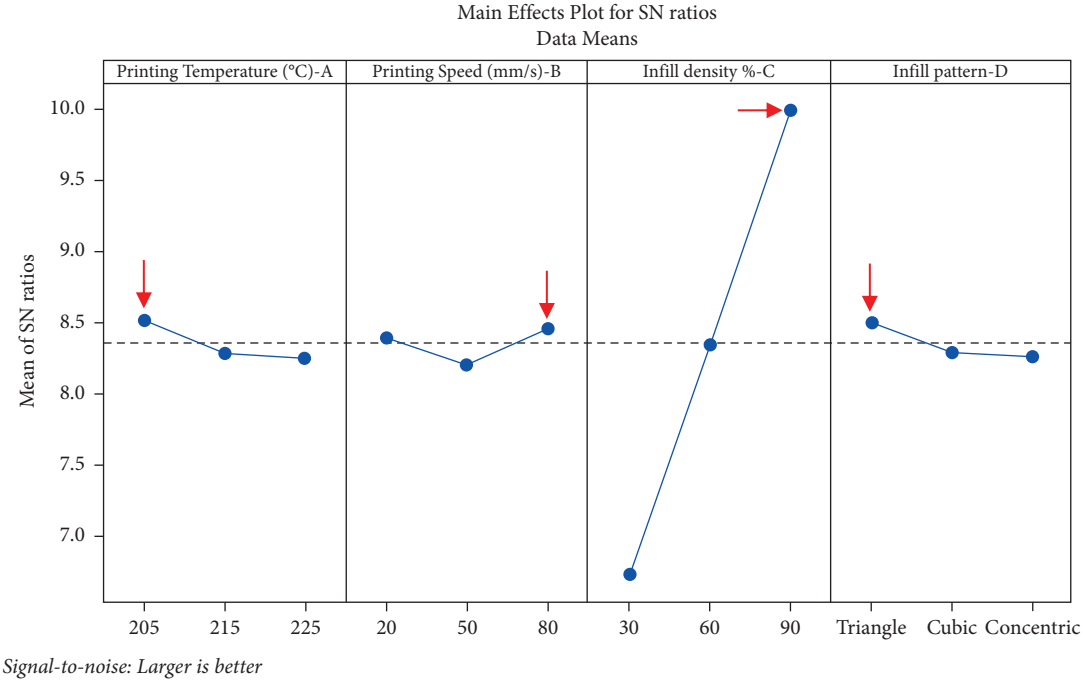

Figure 8: S/N plot of Young's modulus (E).

Table 2 yields the normalized values of the four responses as depicted in Table 9. When the normalized k^{th} response of i^{th} experiment equal or near to one points out that this run is the best regardless of the type response and vice versa for the normalized value equal or approach to zero.

Let us make a sample of calculations for the first value of each response as follows:

$y_1(1)$, max $y_1(1)$, and min $y_1(1)$ = values of the ultimate tensile response are 16, 15, and 24 MPa, respectively.

Then, $x_1(1) = (16 - 15/24 - 15) = 0.11$.

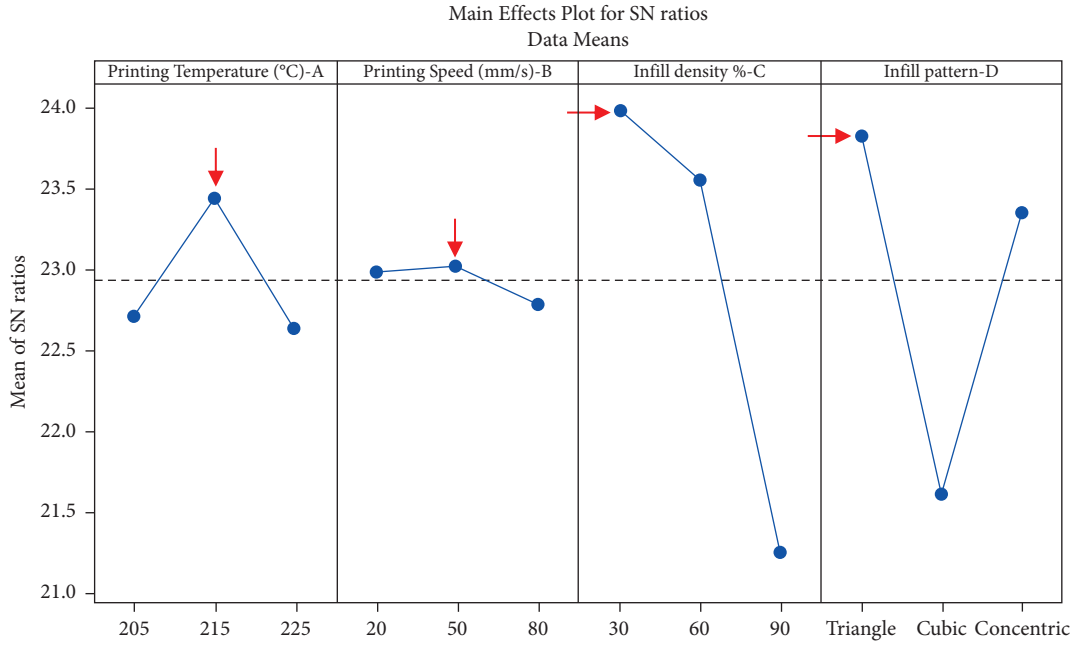

Figure 9: S/N plot of the tensile strain (ε) (%).

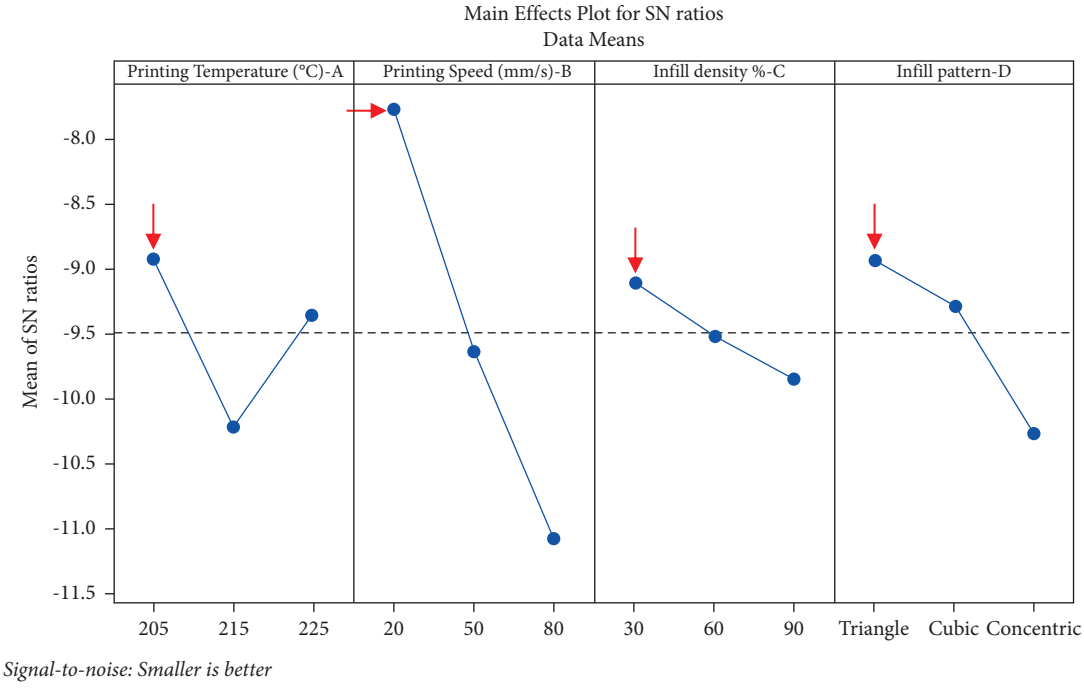

Figure 10: S/N plot of the surface roughness.

Table 8: Optimum 3D printing parameters for each output response.

No.	Output response	Target	Optimum parameters (coded)	Optimum parameters (real values)
1	Ultimate tensile strength σu (MPa)	Maximization	A1B3C3D1	205°C, 80 mm/s, 90%, and triangle pattern
2	Young's modulus of elasticity E (GPa)	Maximization	A1B3C3D1	205°C, 80 mm/s, 90%, and triangle pattern
3	Tensile strain ε (%)	Maximization	A2B2C1D1	215°C, 50 mm/s, 30%, and triangle pattern
4	Surface roughness (Ra)	Minimization	A1B1C1D1	205°C, 20 mm/s, 30%, and triangle pattern

Table 9: Normalized values of tensile strength, Young's modulus, strain, and surface roughness.

Run no.	Ultimate tensile strength (MPa)	Young's modulus (GPa)	Tensile strain (%)	Surface roughness (Ra)
1	0.11	0.15	1	1
2	0.44	0.45	0.41	0.59
3	0.89	1	0.26	0
4	0.33	0.43	0.95	0.51
5	1	0.93	0.54	0.34
6	0	0.07	0.60	0.10
7	0.89	0.90	0	0.78
8	0	0	0.87	0.40
9	0.56	0.5	0.82	0.28

Table 10: Grey relational coefficients (GRCs) and grades (GRGs) of the four responses.

No.	Grey relational coefficients (GRCs)				GRG	Ranking
	Ultimate tensile strength (MPa)	Young's modulus (GPa)	Tensile strain (%)	Surface roughness (Ra)		
1	0.360	0.370	1	1	0.683	2
2	0.474	0.477	0.458	0.546	0.489	7
3	0.818	1	0.403	0.333	0.639	4
4	0.429	0.469	0.910	0.506	0.578	5
5	**1**	**0.876**	**0.518**	**0.431**	**0.706**	**1**
6	0.333	0.350	0.553	0.358	0.399	9
7	0.818	0.837	0.333	0.690	0.670	3
8	0.333	0.333	0.792	0.454	0.478	8
9	0.529	0.502	0.736	0.411	0.545	6

The bold values indicate significant values.

Similarly, for the Young's modulus, tensile strain, and surface roughness, the values are as follows:

$$\begin{aligned} x_1(2) &= \frac{2.26 - 2.09}{3.22 - 2.09} \\ &= 0.15, \\ x_1(3) &= \frac{17.25 - 9.66}{17.25 - 9.66} \\ &= 1, \\ x_1(2) &= \frac{3.81 - 2.05}{3.81 - 2.05} \\ &= 1, \end{aligned} \tag{9}$$

and so on for other values.

After normalization of all response values, the coefficients of grey relational analysis are determined with the aid of the following equation:

$$\gamma(k) = \frac{\Delta \min - \zeta \Delta \min}{\Delta_{0i} + \zeta \Delta \max}, \tag{10}$$

where $\gamma(k)$ represents the grey relational coefficient (GRC), ζ is the distinguishability or identification factor and its value is between 0 and 1 and it is set at 0.5, Δ_{oi} is the absolute difference between the two sequences, and target $x_0(k)$ and comparison target $x_i(k)$, $\Delta \min$, and $\Delta \max$ is the minimum and maximum of Δ_{oi}, respectively.

Finally, the average sum of $\gamma(k)$ (GRC) is calculated by using equation (11) to find the grey relational grade (GRG) as follows:

$$\mathrm{GRG}_i = \frac{1}{n} \sum_{k=1}^{n} \gamma_i(k). \tag{11}$$

Table 10 presents the calculated grey relational coefficients for the four responses, the average GRC, and corresponding rankings.

The table mentioned above illustrates that experiment no. 5 recorded the highest grey relational grade with the first rank. In other words, it is the optimum experimental run that achieved the optimum mechanical properties and surface characteristics with optimized 3D-printing parameters of PLA+ materials. Recalling the parameters and corresponding responses from Table 2 shows the optimum 3D printing parameters as follows: 215°C, 50 mm/s, 90%, and triangle pattern maintained optimum ultimate tensile strength, Young's modulus, tensile strain (24 MPa, 3.14 GPa, and 13.72%), and optimum surface roughness of 3.21 μm. In coded form, the optimum 3D printing parameters that optimized mechanical and surface properties are as follows: A2B2C3D1, where A2 and B2 are the medium levels of printing temperature and speed, while C3 stand for high level of infill density, and finally D1 refers to the triangle pattern. The integrated Taguchi-GRA method proved it is powerful as a multiobjective optimization method.

5. Conclusions

This study dealt with the optimization of 3D-printing parameters to maintain better mechanical properties and surface characteristics of PLA+ materials. Based on the

conducted statistical and parametric analysis besides optimization, the following conclusions were drawn:

(1) The infill density was the most significant parameters in terms of obtained ultimate tensile strength (σu), Young's modulus (E), and tensile strain where it contributed with 96%, 99.09%, and 49.5%, respectively

(2) Pertaining to the surface roughness, it was influenced with printing speed which contributed with 75.67%

(3) The integrated Taguchi-GRA method was able to find the optimum settings for multiple responses together

(4) The optimum settings that ensure optimum mechanical properties and surface characteristic of 24 MPa, 3.14 GPa, 13.72%, and 3.21 μm are medium printing temperature (A2 = 215°C), medium printing speed (B2 = 50 mm/s), high infill density (C3 = 90%), and triangle pattern (D1 = triangle).

(5) The triangle pattern was the best structure for all responses compared with cubic and concentric patterns.

Data Availability

The data that support the findings of the study are available from the corresponding author upon request.

Conflicts of Interest

The authors declare that they have no conflicts of interest.

References

[1] N. M. Abdulkhaleq and M. M. Ghareeb, "Combination of FDM 3D printing and compressed tablet for preparation of baclofen as gastro-floating drug delivery system (conference paper)#," *Iraqi Journal of Pharmaceutical Sciences*, vol. 31, pp. 18–24, 2023.

[2] A. Majeed, Y. Zhang, S. Ren et al., "A big data-driven framework for sustainable and smart additive manufacturing," *Robotics and Computer-Integrated Manufacturing*, vol. 67, Article ID 102026, 2021.

[3] R. Kleer and F. T. Piller, "Local manufacturing and structural shifts in competition: market dynamics of additive manufacturing," *International Journal of Production Economics*, vol. 216, pp. 23–34, 2019.

[4] U. Fasel, D. Keidel, L. Baumann, G. Cavolina, M. Eichenhofer, and P. Ermanni, "Composite additive manufacturing of morphing aerospace structures," *Manufacturing Letters*, vol. 23, pp. 85–88, 2020.

[5] E. Rezvani Ghomi, F. Khosravi, R. E. Neisiany, S. Singh, and S. Ramakrishna, "Future of additive manufacturing in healthcare," *Current Opinion in Biomedical Engineering*, vol. 17, Article ID 100255, 2021.

[6] J. Boer, W. Lambrechts, and H. Krikke, "Additive manufacturing in military and humanitarian missions: advantages and challenges in the spare parts supply chain," *Journal of Cleaner Production*, vol. 257, Article ID 120301, 2020.

[7] D. Assante, G. M. Cennamo, and L. Placidi, "3D printing in education: an European perspective," in *Proceedings of the IEEE Global Engineering Education Conference (EDUCON)*, Porto, Portugal, April 2020.

[8] B. Ameri, F. Taheri-Behrooz, and M. R. M. Aliha, "Fracture loads prediction of the modified 3D-printed ABS specimens under mixed-mode I/II loading," *Engineering Fracture Mechanics*, vol. 235, Article ID 107181, 2020.

[9] Z. Al-Dulimi, M. Wallis, D. K. Tan, M. Maniruzzaman, and A. Nokhodchi, "3D printing technology as innovative solutions for biomedical applications," *Drug Discovery Today*, vol. 26, no. 2, pp. 360–383, 2021.

[10] S. Petersmann, M. Spoerk, W. Van De Steene et al., "Mechanical properties of polymeric implant materials produced by extrusion-based additive manufacturing," *Journal of the Mechanical Behavior of Biomedical Materials*, vol. 104, Article ID 103611, 2020.

[11] R. Auras, "Poly(lactic acid)," in *Encyclopedia of Polymer Science and Technology*, Wiley, Hoboken, NJ, USA, 2010.

[12] V. DeStefano, S. Khan, and A. Tabada, "Applications of PLA in modern medicine," *Engineered Regeneration*, vol. 1, pp. 76–87, 2020.

[13] S. Castañeda-Rodríguez, M. González-Torres, R. M. Ribas-Aparicio et al., "Recent advances in modified poly (lactic acid) as tissue engineering materials," *Journal of Biological Engineering*, vol. 17, no. 1, p. 21, 2023.

[14] C. Bellehumeur, L. Li, Q. Sun, and P. Gu, "Modeling of bond formation between polymer filaments in the fused deposition modeling process," *Journal of Manufacturing Processes*, vol. 6, no. 2, pp. 170–178, 2004.

[15] A. S. Baden, "Optimization and prediction of process parameters in SPIF that affecting on surface quality using simulated annealing algorithm," *Al-Khwarizmi Engineering Journal*, vol. 12, no. 4, pp. 81–92, 2017.

[16] M. Leite, "Study of the influence of 3d printing parameters on the mechanical properties of pla," in *Proceedings of the 3rd International Conference on Progress in Additive Manufacturing (Pro-AM 2018)*, Singapore, May 2018.

[17] V. D. Sagias, K. I. Giannakopoulos, and C. Stergiou, "Mechanical properties of 3D printed polymer specimens," *Procedia Structural Integrity*, vol. 10, pp. 85–90, 2018.

[18] F. G. Christian and P. Ezekielle, "Mechanical characterisation of photopolymer resins for rapid prototyping," in *Proceedings of the 27th Danubia Adria Symposium on Experimental Solid Mechanics*, Wroclaw University of Technology, Wroclaw, Poland, March 2010.

[19] A. Čikmiš, "the process of developing conceptual design of a product using rapid prototyping technology," in *Proceedings of the 18th International Research/Expert Conference"Trends in the Development of Machinery and Associated Technology"TMT 2014*, Budapest, Hungary, September 2014.

[20] S. H. Ahn, M. Montero, D. Odell, S. Roundy, and P. K. Wright, "Anisotropic material properties of fused deposition modeling ABS," *Rapid Prototyping Journal*, vol. 8, no. 4, pp. 248–257, 2002.

[21] B. Mueller, "Additive manufacturing technologies – rapid prototyping to direct digital manufacturing," *Assembly Automation*, vol. 32, no. 2, 2012.

[22] K. Dotchev, "Rapid prototyping and engineering applications: a toolbox for prototype development," *Assembly Automation*, vol. 29, no. 3, 2009.

[23] N. G. Tanikella, B. Wittbrodt, and J. M. Pearce, "Tensile strength of commercial polymer materials for fused filament fabrication 3D printing," *Additive Manufacturing*, vol. 15, pp. 40–47, 2017.

[24] S. Anand Kumar and Y. Shivraj Narayan, "Tensile testing and evaluation of 3D-printed PLA specimens as per ASTM D638 type IV standard," in *Innovative Design, Analysis and Development Practices in Aerospace and Automotive Engineering (I-DAD 2018)*, Springer Singapore, Singapore, 2019.

[25] C. Lubombo and M. A. Huneault, "Effect of infill patterns on the mechanical performance of lightweight 3D-printed cellular PLA parts," *Materials Today Communications*, vol. 17, pp. 214–228, 2018.

[26] N. A. Ali, "Characterization of biochar (bio carbon) on the properties of plasticized polylactic acid composites for antistatic packaging," *Iraqi Journal of Physics*, vol. 17, no. 42, pp. 13–26, 2019.

[27] M. Alhazmi and A. Backar, *Influence of Infill Density and Orientation On the Mechanical Response of Pla+ Specimens Produced Using FDM 3D Printing*, Umm Al-Qura University, Mecca, Saudi Arabia, 2020.

[28] S. Kain, J. V. Ecker, A. Haider, M. Musso, and A. Petutschnigg, "Effects of the infill pattern on mechanical properties of fused layer modeling (FLM) 3D printed wood/polylactic acid (PLA) composites," *European Journal of Wood and Wood Products*, vol. 78, no. 1, pp. 65–74, 2020.

[29] B. Aloyaydi, S. Sivasankaran, and A. Mustafa, "Investigation of infill-patterns on mechanical response of 3D printed polylactic-acid," *Polymer Testing*, vol. 87, Article ID 106557, 2020.

[30] A. A. Al-Tamimi, H. Almeida, and P. Bartolo, "Structural optimisation for medical implants through additive manufacturing," *Progress in Additive Manufacturing*, vol. 5, no. 2, pp. 95–110, 2020.

[31] W. Qiu, P. Jin, S. Jin et al., "An evolutionary design approach to shell-infill structures," *Additive Manufacturing*, vol. 34, Article ID 101382, 2020.

[32] J. Alexandersen and C. S. Andreasen, "A review of topology optimisation for fluid-based problems," *Fluid*, vol. 5, no. 1, p. 29, 2020.

[33] J. M. Chacón, M. Caminero, E. García-Plaza, and P. Núñez, "Additive manufacturing of PLA structures using fused deposition modelling: effect of process parameters on mechanical properties and their optimal selection," *Materials and Design*, vol. 124, pp. 143–157, 2017.

[34] K. A. Monogarov, I. V. Fomenkov, and A. N. Pivkina, "FDM 3D printing of combustible structures: first results," *Mendeleev Communications*, vol. 32, no. 2, pp. 228–230, 2022.

[35] S. Maurya, B. Malik, P. Sharma, A. Singh, and R. Chalisgaonkar, "Investigation of different parameters of cube printed using PLA by FDM 3D printer," *Materials Today: Proceedings*, vol. 64, pp. 1217–1222, 2022.

[36] M. Doshi, A. Mahale, S. Kumar Singh, and S. Deshmukh, "Printing parameters and materials affecting mechanical properties of FDM-3D printed Parts: perspective and prospects," *Materials Today: Proceedings*, vol. 50, pp. 2269–2275, 2022.

[37] R. Phillip, "Parameter and tolerance design," *Taguchi Techniques for Quality Engineering: Loss Function*, McGraw-Hill, New York, NY, USA, 2nd edition, 1995.

[38] D. C. Montgomery, *Design and Analysis of Experiments*, Springer, Singapore, 10th edition, 2020.

[39] A. Milovanović, A. Sedmak, A. Grbović et al., "Comparative analysis of printing parameters effect on mechanical properties of natural PLA and advanced PLA-X material," *Procedia Structural Integrity*, vol. 28, pp. 1963–1968, 2020.

[40] M. Mia, M. A. Khan, S. S. Rahman, and N. R. Dhar, "Mono-objective and multi-objective optimization of performance parameters in high pressure coolant assisted turning of Ti-6Al-4V," *The International Journal of Advanced Manufacturing Technology*, vol. 90, no. 1-4, pp. 109–118, 2017.

[41] Y. Kuo, T. Yang, and G.-W. Huang, "The use of a grey-based Taguchi method for optimizing multi-response simulation problems," *Engineering Optimization*, vol. 40, no. 6, pp. 517–528, 2008.